Progress In Electromagnetics Research, PIER 47, 313–333, 2004

REDUCTION OF ERRORS IN ANTENNA RADIATION PATTERNS USING OPTIMALLY TRUNCATED SPHERICAL WAVE EXPANSION

P. Koivisto

VTT Information Technology
Telecommunications
P.O. Box 1202, FIN-02044 VTT, Finland

Abstract—This paper demonstrates how the error of a measured or simulated antenna radiation pattern can be decreased by calculating a spherical wave expansion (SWE) with an optimised truncation mode index. Four radiation pattern examples are examined for which the analytical expression of the electrical field is known. Upon adding random and ϕ-alignment errors to the exact electric fields, the SWEs are determined and compared with the corresponding ones for the exact fields. These comparisons show that the accuracy of the calculated SWE is much better than the accuracy of the original inaccurate field. Resting on the calculated examples, a method is created which can be used to determine the optimal truncation index from the modal power distribution of a SWE without knowing the exact field. Finally, the method developed is applied to measured antenna radiation patterns.

1 Introduction

2 Theory, Definitions and Description of Considered Examples

2.1 Representation and Calculation of Coefficients of a Spherical Wave Expansion

2.2 Characteristic Modal Power Distribution

2.3 Antenna Examples

2.4 Error

3 SWE Calculations

3.1 Behaviour of Modal Power Distribution

3.2 Error of the Calculated SWE

3.3 Optimal Truncation Indices

4 Calculation of the Optimal Truncation Index from Measured Data
4.1 Method to Find the Optimal Truncation Index
4.2 Application to Measured Radiation Patterns
5 Conclusions
References

1. INTRODUCTION

The spherical wave expansion (SWE) is an accurate and convenient way to represent a complete 3-D radiation pattern of an antenna. Once the coefficients of the SWE are known, the complex amplitudes of both electric field components can be calculated everywhere outside the origin-centred smallest sphere enclosing the antenna. Although an accurate SWE contains, in principle, an infinite number of modes, a reasonably small number of lowest modes are enough in all practical problems, because the expansion, owing to the feature of spherical Hankel functions, converges rather quickly with increasing mode index for large mode indices. Thus, the SWE can be truncated at a relatively low mode index N without a substantial error.

The topic of a proper truncation mode index N has been discussed previously in the literature, but so far, only the truncation error of the expansion has been taken into account, while the possible errors of the data itself have been ignored. Various empirical and semi-empirical rules for N have been given in references [1–3]. In an earlier paper by this author [4] analytical expressions for the characteristic modal power distribution and truncation error as a function of N have been derived. The appropriate truncation index N as a function of the desired accuracy and antenna size can be determined using the expression for the truncation error. Contrary to the earlier papers, here the error of data has also been considered while determining the optimal truncation index for the SWE. In contrast to error-free data, the increase of the number of terms in the expansion does not necessarily lead to a more accurate representation.

In practical measurements, there exists a large amount of various error sources [5]. Besides unwanted reflections, scattering and signal leakage also inexactness of antenna alignment degrade the accuracy of a measurement. Numerous different methods to reduce such errors are described in the literature, for instance, antenna alignment errors are discussed in [7]. A plane wave, pattern subtraction range compensation method is described in reference [6], where also other techniques

to compensate for range-field induced radiation pattern errors are presented. Two of those methods are based on SWEs [8, 9]. The purpose of this paper is to examine how much radiation pattern errors can be reduced merely by calculating the SWE with the best possible truncation index.

While the accurate field is unknown in practical radiation pattern measurements, simulated numerical examples representing inaccurate measured radiation patterns are examined. By means of these examples, the dependencies of the optimal truncation index and the decrease of error on the error level and type are examined. These results make it possible to develop a method to find the optimal truncation index even when the exact pattern is not known.

2. THEORY, DEFINITIONS AND DESCRIPTION OF CONSIDERED EXAMPLES

2.1. Representation and Calculation of Coefficients of a Spherical Wave Expansion

A few slightly different ways to express the SWE are used in the literature [1, 10–12]. In this paper the SWE for the electric and magnetic fields outside the smallest possible origin centred sphere enclosing the source ($r > r_0$) is given by

$$\boldsymbol{E}(r,\theta,\phi) = \sum_{n=1}^{\infty}\sum_{m=-n}^{n}\left[a_{mn}\boldsymbol{M}_{mn}(r,\theta,\phi) + b_{mn}\boldsymbol{N}_{mn}(r,\theta,\phi)\right] \quad (1)$$

$$\boldsymbol{H}(r,\theta,\phi) = \frac{jk}{\omega\mu}\sum_{n=1}^{\infty}\sum_{m=-n}^{n}\left[b_{mn}\boldsymbol{M}_{mn}(r,\theta,\phi) + a_{mn}\boldsymbol{N}_{mn}(r,\theta,\phi)\right] \quad (2)$$

where $k = \omega\sqrt{\varepsilon\mu} = 2\pi/\lambda$ is the wave number. The vectors $\boldsymbol{M}$ and $\boldsymbol{N}$, called vector spherical wave functions, are defined by

$$\begin{aligned}\boldsymbol{M}_{mn}(r,\theta,\phi) &= \nabla\times(\boldsymbol{r}\psi_{mn})\\ \boldsymbol{N}_{mn}(r,\theta,\phi) &= k^{-1}\nabla\times\nabla\times(\boldsymbol{r}\psi_{mn})\end{aligned} \quad (3)$$

where the scalar spherical wave functions for outward travelling fields are

$$\psi_{mn}(r,\theta,\phi) = e^{-jm\phi}h_n^{(2)}(kr)P_n^{|m|}(\cos\theta). \quad (4)$$

In these expressions, the functions $P_n^{|m|}$ are the associated Legendre functions and $h_n^{(2)}$ are the spherical Hankel functions of the second kind.

Using the asymptotic form of the spherical Hankel functions the electric field components in the far-field region can be expressed as

$$
\begin{aligned}
E_\theta &= \sum_{n=1}^{\infty} \sum_{m=-n}^{n} \left[a'_{mn}(-jm) \frac{P_n^{|m|}(\cos\theta)}{\sin\theta} + b'_{mn} \frac{dP_n^{|m|}(\cos\theta)}{d\theta} \right] \exp(-jm\phi) \\
E_\phi &= \sum_{n=1}^{\infty} \sum_{m=-n}^{n} \left[a'_{mn} \left(-\frac{dP_n^{|m|}(\cos\theta)}{d\theta} \right) + b'_{mn}(-jm) \frac{P_n^{|m|}(\cos\theta)}{\sin\theta} \right] \exp(-jm\phi) \\
E_r &= 0
\end{aligned} \tag{5}
$$

where

$$
\begin{aligned}
a'_{mn} &= a_{mn} h_n^{(2)}(kr) = j^{n+1} \frac{e^{-jkr}}{kr} a_{mn} \\
b'_{mn} &= b_{mn} \frac{1}{kr} \frac{d}{d(kr)} \left[h_n^{(2)}(kr) kr \right] = j^n \frac{e^{-jkr}}{kr} b_{mn}
\end{aligned}
$$

Calculation routines based on these formulas have been implemented in Matlab and are used in all the examples of this paper. The complex coefficients a'_{mn}, b'_{mn} of the expansion were calculated using the matrix division function included in Matlab: The vector containing complex θ- and ϕ-components of the electric field at several directions is divided by the matrix composed of the values of the functions corresponding to each coefficient at the respective directions and the given data. The matrix division finds the least squares solution to the system of linear equations expressed by the matrix and the data vector.

The number of obtainable coefficients in the SWE, when calculated from error-free data, depends on the number of data points and their spatial arrangement. The definite maximum for the number of coefficients is fixed by the number of data points, but a systematic configuration of the data decreases the number of coefficients in the best possible expansion. Expression (1) for SWE reveals that an expansion truncated at the mode index N includes $J = 2N(N+2)$ modes. While each coefficient and both field components are complex numbers, the number of coefficients must be less or equal to two times the number of field points M ($J \leq 2M$), which leads to the condition $N \leq \sqrt{M+1} - 1$.

Consider a radiation pattern data where the field points are distributed along n_ϕ constant ϕ-cuts ($0 \leq \phi < \pi$) around the antenna, in such a way that for each $2n_\phi$ ϕ-values ($0 \leq \phi < 2\pi$) the θ-values ($0 \leq \theta < \pi$) are the same. In that case the number of ϕ-cuts (n_ϕ) and θ-values (n_θ) set an upper limit for the truncation index. If N exceed either n_ϕ or n_θ, the accuracy of the expansion decreases even with

accurate data. Although coincidence between the data and the field given by the expansion improves at the data points, when N exceeds n_ϕ or n_θ, it becomes worse everywhere else. Thus, the average accuracy of the expansion decreases. Consequently, a rule for optimal truncation index for error-free data is given by

$$N_{opt,exact} = \min\left\{n_\phi, n_\theta, \sqrt{M+1} - 1\right\}. \tag{6}$$

2.2. Characteristic Modal Power Distribution

A modal power distribution $P(n)$ of a SWE is defined as the proportion of the radiated power in modes with index n to the total radiated power. It is advantageous to use the logarithmic form of the modal power distribution, which is

$$P(n)[dB] = 10\log(P(n)) = 10\log\left(\frac{\sum_{m=-n}^{n}\left(P_{mn}^{TE}+P_{mn}^{TM}\right)}{\sum_{n=1}^{\infty}\sum_{m=-n}^{n}\left(P_{mn}^{TE}+P_{mn}^{TM}\right)}\right) \tag{7}$$

where

$$\begin{aligned} P_{mn}^{TE} &= \frac{\pi|a_{mn}|^2}{\eta k^2}\frac{2n(n+1)}{2n+1}\frac{(n+|m|)!}{(n-|m|)!} \\ P_{mn}^{TM} &= \frac{\pi|b_{mn}|^2}{\eta k^2}\frac{2n(n+1)}{2n+1}\frac{(n+|m|)!}{(n-|m|)!} \end{aligned} \tag{8}$$

are the powers of the radiated field in each mode.

The characteristic modal power distribution of an antenna is a modal power distribution whose shape only depends on the size kr_0 of the antenna. An analytical expression for it has been derived in [4] from the assumption of equal average amplitude for each mode over the surface of the minimum sphere enclosing the antenna [1]. Integrating the square of the electric field amplitude of each mode in the near-field expansion (1) over the surface of the minimum sphere, dividing the result by 4π and taking the square root gives the average amplitudes per solid angle at r_0

$$\begin{aligned} \left|\boldsymbol{E}_{mn}^{TE}\right|_{ave} &= \left|h_n^{(2)}(kr_0)a_{mn}\right|\sqrt{\frac{n(n+1)}{2n+1}\frac{(n+|m|)!}{(n-|m|)!}} \\ &= \sqrt{\frac{\eta}{2\pi}}k\left|h_n^{(2)}(kr_0)\right|\sqrt{P_{mn}^{TE}} \end{aligned}$$

$$\left|\boldsymbol{E}_{mn}^{TM}\right|_{ave} = \left|\left(\frac{1}{kr}\frac{\mathrm{d}\left(krh_n^{(2)}(kr)\right)}{\mathrm{d}(kr)}\right)\right|_{r=r_0} b_{mn}\left|\sqrt{\frac{n(n+1)}{2n+1}\frac{(n+|m|)!}{(n-|m|)!}}\right.$$
$$= \sqrt{\frac{\eta}{2\pi}}k\left|\left(\frac{1}{kr}\frac{\mathrm{d}\left(krh_n^{(2)}(kr)\right)}{\mathrm{d}(kr)}\right)\right|_{r=r_0}\sqrt{P_{mn}^{TM}} \quad (9)$$

By equating these average amplitudes the relations between the powers in each mode

$$P_{mn}^{TE} = \frac{\left|h_1^{(2)}(kr_0)\right|^2}{\left|h_n^{(2)}(kr_0)\right|^2}P_{01}^{TE} \qquad P_{mn}^{TM} = \frac{\left|h_1^{(2)}(kr_0)\right|^2}{\left|h_{n-1}^{(2)}(kr_0) - n\dfrac{h_n^{(2)}(kr_0)}{kr_0}\right|^2}P_{01}^{TE} \quad (10)$$

are obtained. Inserting these into the expression (7) leads to an expression for the logarithmic characteristic modal power distribution

$$P_c(n)[dB] = 10\log\left(\frac{(2n+1)\left(\left|h_n^{(2)}(kr_0)\right|^{-2} + \left|h_{n-1}^{(2)}(kr_0) - n\dfrac{h_n^{(2)}(kr_0)}{kr_0}\right|^{-2}\right)}{\displaystyle\sum_{l=1}^{\infty}(2l+1)\left(\left|h_l^{(2)}(kr_0)\right|^{-2} + \left|h_{l-1}^{(2)}(kr_0) - l\dfrac{h_l^{(2)}(kr_0)}{kr_0}\right|^{-2}\right)}\right) \quad (11)$$

2.3. Antenna Examples

Four different idealized antenna configurations will be considered in the following. The geometry of configurations 1 and 2 is similar and represented in Figure 1a. They consist of two elementary electric dipoles lying on the z-axis, a z directed at $z = r_0$ and an x-directed at $z = -r_0$ and two elementary magnetic dipoles lying on the y-axis, a z directed at $y = r_0$ and an x-directed at $y = -r_0$. Since all the dipoles are in the same phase, the electric field components of these antennas are

$$E_\theta \propto -\sin\theta e^{jkr_0\cos\theta} + \cos\theta\cos\phi e^{-jkr_0\cos\theta} - \sin\phi e^{-jkr_0\sin\theta\sin\phi}$$
$$E_\phi \propto -\sin\phi e^{-jkr_0\cos\theta} + \sin\theta e^{jkr_0\sin\theta\sin\phi} - \cos\theta\cos\phi e^{-jkr_0\sin\theta\sin\phi} \quad (12)$$

In configuration 1 $kr_0 = \pi/5$, while $kr_0 = \pi/2$ in configuration 2.

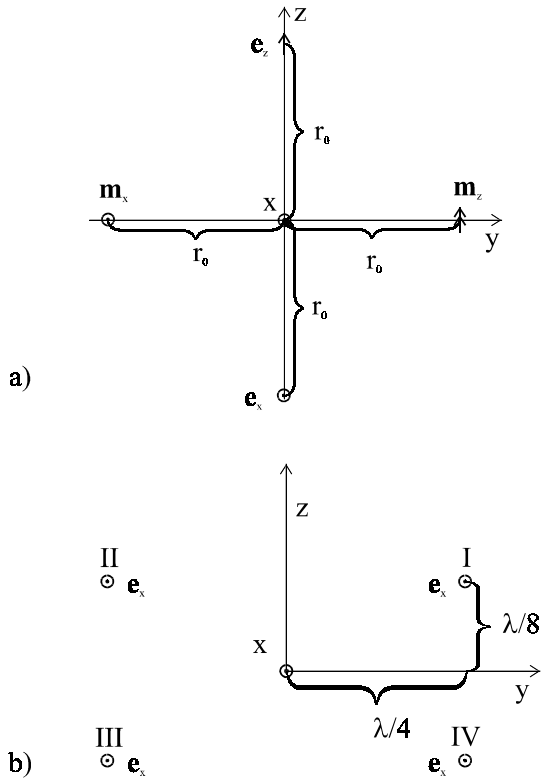

Figure 1. Arrangement of elementary electric (**e**) and magnetic (**m**) dipoles in the antenna configurations 1-2 (figure a) and 3-4 (figure b).

Antenna configurations 3 and 4, shown in Figure 1b, consist of four x-directed elementary electric dipoles in the y-z-plane at $(y, z) = (\pm\lambda/4, \pm\lambda/8)$, so that $kr_0 = \pi\sqrt{5}/4$. In the antenna configuration 3, dipoles I and II as well as dipoles III and IV are mutually in the same phase while between dipole III and I the phase shift is $\pi/2$. Then, the electric field components are

$$\begin{aligned} E_\theta &\propto \cos\theta\cos\phi\cos\left(\frac{\pi}{2}\sin\theta\sin\phi\right)\cos\left(\frac{\pi}{4}(\cos\theta-1)\right) \\ E_\phi &\propto -\sin\phi\cos\left(\frac{\pi}{2}\sin\theta\sin\phi\right)\cos\left(\frac{\pi}{4}(\cos\theta-1)\right) \end{aligned} \tag{13}$$

In the antenna configuration 4, the phase shift between dipole I and IV is $\pi/2$ while dipoles I and III as well as II and IV are in the same

phase. Thus the electric field components are

$$\begin{aligned} E_\theta &\propto \cos\theta\cos\phi\left\{\cos\left(\frac{\pi}{2}\sin\theta\sin\phi\right)\cos\left(\frac{\pi}{4}\cos\theta\right)\right. \\ &\quad \left. - j\sin\left(\frac{\pi}{2}\sin\theta\sin\phi\right)\sin\left(\frac{\pi}{4}\cos\theta\right)\right\} \\ E_\phi &\propto -\sin\phi\left\{\cos\left(\frac{\pi}{2}\sin\theta\sin\phi\right)\cos\left(\frac{\pi}{4}\cos\theta\right)\right. \\ &\quad \left. - j\sin\left(\frac{\pi}{2}\sin\theta\sin\phi\right)\sin\left(\frac{\pi}{4}\cos\theta\right)\right\} \end{aligned} \tag{14}$$

The power radiation patterns for all the four antennas are shown in Figure 2.

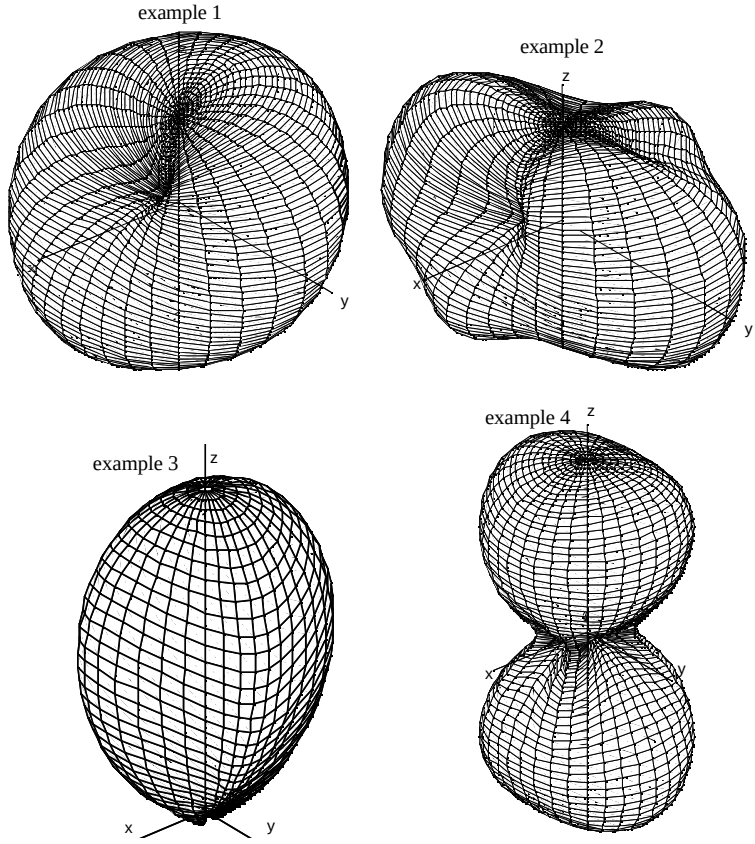

Figure 2. Total power radiation patterns of the four antennas.

2.4. Error

In this paper, the error of a field is defined as the rms. difference between the exact (E^{ex}) and inaccurate (E) fields normalised by the average amplitude of the exact field ($\tilde{E}^{ex}$). It is expressed by the formula

$$\delta_E = \left[\frac{1}{M} \sum_{k=1}^{M} \left\{ \left| E_{\theta k}^{ex} - E_{\theta k} \right|^2 + \left| E_{\phi k}^{ex} - E_{\phi k} \right|^2 \right\} \Big/ \left(\tilde{E}^{ex} \right)^2 \right]^{1/2} \tag{15}$$

where the index k runs through all the M directions where the field components are known and the average amplitude of the exact field is calculated as

$$\left(\tilde{E}^{ex} \right)^2 = \frac{1}{4\pi} \int_0^{\pi} \int_0^{2\pi} \left(\left| E_{\theta}^{ex}(\theta, \phi) \right|^2 + \left| E_{\phi}^{ex}(\phi, \phi) \right|^2 \right) \sin\theta d\theta d\theta.$$

Two different kinds of errors are examined: random error and error caused by misalignment in fixing the ϕ-cut. The random error was generated by adding a small normally distributed random variable to the real- and imaginary parts of each field component. In the following examples, standard deviation of the added quantity was set in such a way that the error level of the data, expressed by equation (15), is 0.10, 0.05, 0.02, 0.01 and 0.001. The ϕ-error data is obtained by calculating the fields for each cut with ϕ value, which differs slightly from the right one. In the examples, the angle error varies randomly between $\pm 1^\circ$ and $\pm 2^\circ$. Typical examples of both kinds of error are illustrated in Figure 3, where the squared amplitude of the difference between the inaccurate and exact fields is drawn. These figures show the characteristics of the two kinds of errors. As expected, random errors of real and imaginary parts lead to random differences in the amplitude, while errors due to misalignments of the ϕ-cuts behave regularly.

3. SWE CALCULATIONS

The SWEs were calculated using the numerically generated inaccurate fields as data, and the fields given by the expansions were compared with the original exact field using the error formula (15). These calculations were carried out with different truncation mode indices N and number of field data directions M. The amount of data directions was 1620 ($\theta = 1^\circ, 3^\circ \ldots 179^\circ$ & $\phi = 0^\circ, 20^\circ \ldots 340^\circ$), 3240 ($\theta = 1^\circ, 3^\circ \ldots 179^\circ$ & $\phi = 0^\circ, 10^\circ \ldots 350^\circ$), 6480 ($\theta = 1^\circ, 3^\circ \ldots 179^\circ$ & $\phi = 0^\circ, 5^\circ \ldots 355^\circ$) and 12960 ($\theta = 1^\circ, 2^\circ \ldots 180^\circ$ & $\phi = 0^\circ, 5^\circ \ldots 355^\circ$). In

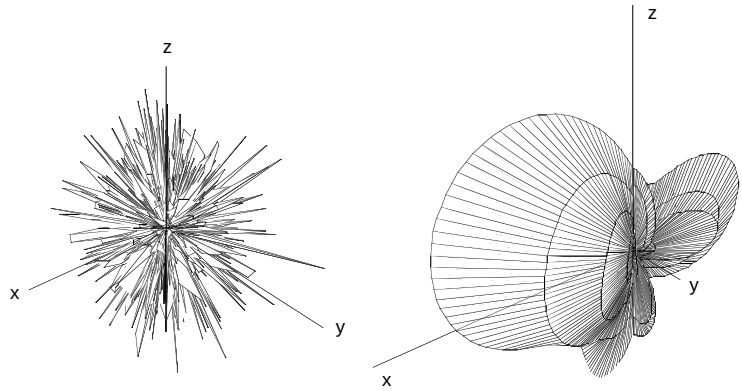

Figure 3. Typical spatial error distributions for random a) and ϕ-angle alignment b) field errors, shown as squared amplitude of difference between inaccurate and exact fields.

all cases, the number of the ϕ-cuts was at least 9, which is not exceed by the optimum truncation index. Thus, the truncation index is limited only by the inaccuracy of the field, and the effect of number of the ϕ-cuts need not be considered.

3.1. Behaviour of Modal Power Distribution

In [4] it has been shown that the modal power distribution of an antenna follows rather well the corresponding characteristic modal power distribution, depending only on the value of kr_0. Figure 4 and Figure 5 show a few examples of the modal power distributions for the calculated SWEs with antenna configurations 1 and 3. In Figure 4 the random error levels are 0.1 and 0.01, while Figure 5 shows results for the ϕ-alignment error. The corresponding characteristic modal power distributions for both antennas are also shown. The distributions of the expansions display a flat region on the high mode indices, while the characteristic distributions decrease more and more steeply with increasing mode index. In addition, the mode index at which the flat part begins and its level depend on the error level and the number of data points. At mode indices below the flat part, the calculated and characteristic distributions follow each other reasonably well. Comparing the distributions for all the four antennas reveals that the level of the flat part does not depend much on the kr_0 value. Since the rate of fall of the characteristic distribution decrease with increasing kr_0, the turning point of the modal power distribution depends on kr_0: the larger kr_0, the higher is the mode index where

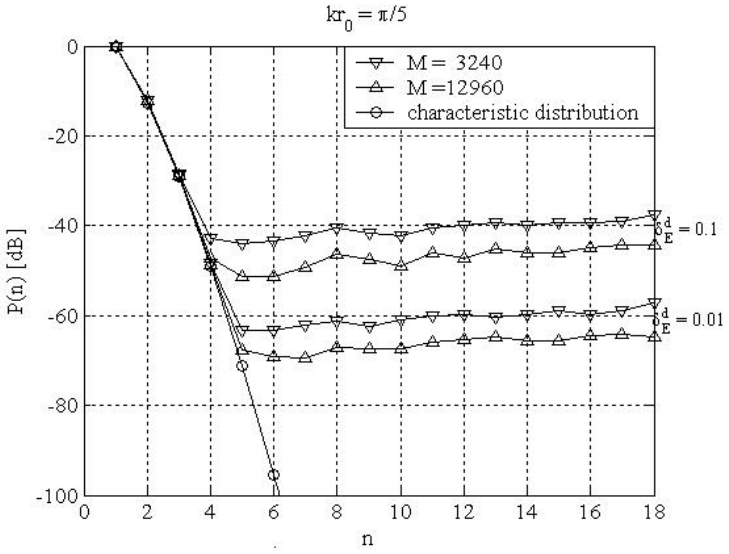

(a)

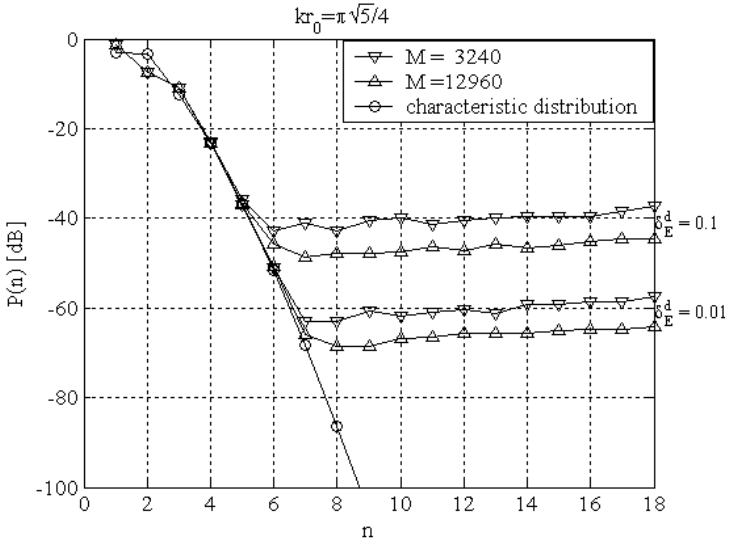

(b)

Figure 4. Modal power distributions for SWEs calculated with truncation mode index $N = 18$ with the corresponding characteristic distributions. The SWEs were calculated from field data with random errors 0.1 and 0.01 for antenna examples 1 (figure a) and 3 (figure b).

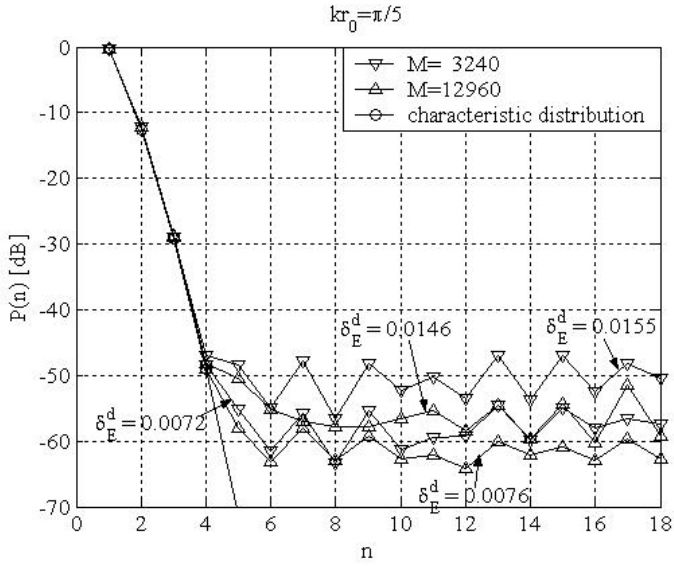

(a)

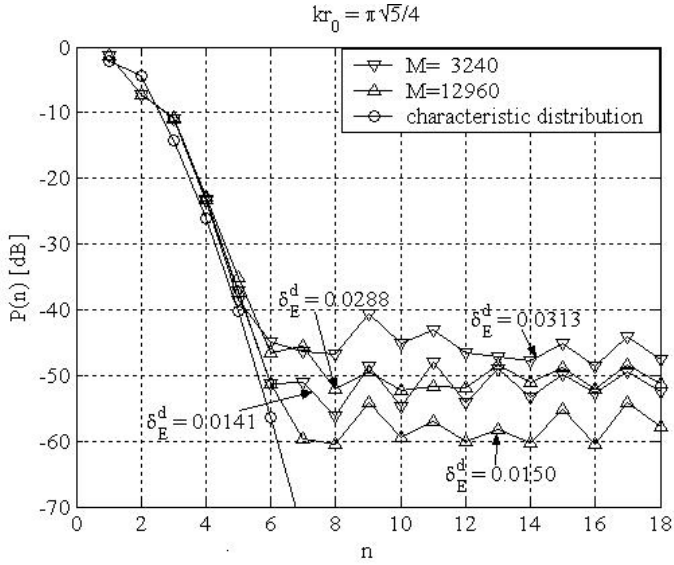

(b)

Figure 5. Same as Figure 4 when the SWEs were calculated from field data with ϕ-alignment errors.

the flat part begins.

The different behaviour of the calculated SWE and characteristic power distribution suggests that the calculated SWE on those modes with the indices on the flat region consist mainly of the error in the field data. Thus, one can assume that it would be preferable to truncate the expansion near the mode index where the flat part starts.

3.2. Error of the Calculated SWE

Figure 6 and Figure 7 show the errors of the SWEs calculated from the data with random and ϕ-alignment errors as a function of the truncation mode index. The results prove that there is indeed an optimal truncation mode index, which minimises error of the expansion. In addition, it lies near the turning point of the modal power distribution, where the distribution for the SWE begins to deviate from the characteristic one. Naturally, for very small truncation indices, the error level of the expansion can be even higher than the error of the data used. However, at and near the optimal truncation index, the errors of the SWEs are much smaller than the error of the data used. Above the optimal truncation index the errors increase only gradually, approaching the level of data error but remaining clearly below it.

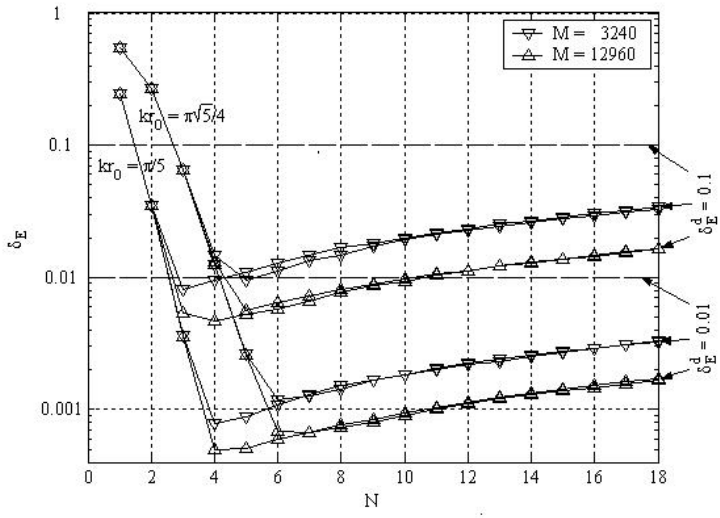

Figure 6. Error of SWEs as a function of truncation mode index. SWEs were calculated from data with random error.

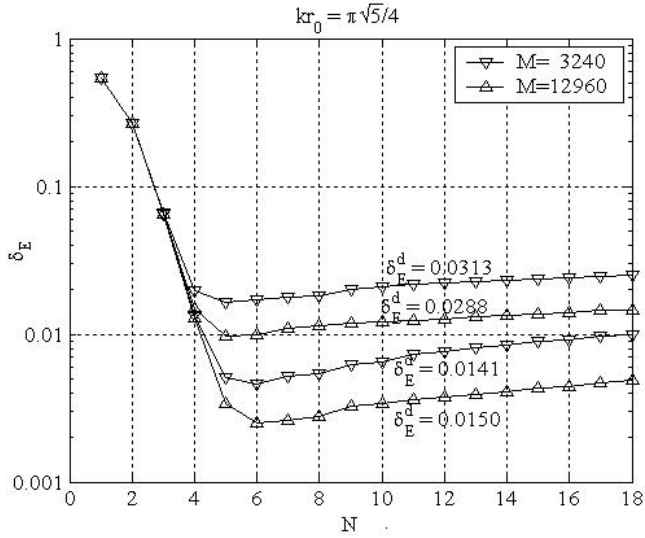

Figure 7. Error of SWEs as a function of truncation mode index. SWEs were calculated from data with ϕ-alignment error.

Figure 8 illustrates the reduction of the error level achieved by calculating the SWE with the optimal truncation index. Although both error types were clearly decreased, the figure reveals an essential difference between the two types. While 80–95 percent of the random error was eliminated, only about 30 to 80 percent of the error due to the ϕ-misalignment was removed. Dependence of the error on the number of data can clearly be seen: the proportion of the remaining error to the data error decreases with an increasing number of data.

3.3. Optimal Truncation Indices

The optimal truncation indices for all antenna examples and random errors are given in Table 1. These figures show that the optimal truncation index increases with increasing kr_0 and the number of data, and with decreasing error of data. Same dependencies also apply for the optimal truncation indices given in Table 2, which are calculated for the data with the ϕ-alignment error. The optimal truncation indices for both error types with equal data errors are roughly the same. Only in a few cases the ϕ-alignment errors leads to a lower truncation index.

Table 1. Optimal truncation mode indices for SWEs calculated from the data with random error.

	example 1, $kr_0 = \pi/5 \approx 0.628$				example 2, $kr_0 = \pi/2 \approx 1.571$			
δ_E^d \ M	1620	3240	6480	12960	1620	3240	6480	12960
0.1	3	3	3	4	5	5	5	5
0.05	4	4	4	4	5	5	5	5
0.02	4	4	4	4	5	6	6	6
0.01	4	4	4	4	6	6	6	6
0.001	5	5	5	5	7	7	7	7
	example 3, $kr_0 = \pi\sqrt{5}/4 \approx 1.756$				example 4, $kr_0 = \pi\sqrt{5}/4 \approx 1.756$			
0.1	5	5	5	5	5	5	5	5
0.05	5	5	6	6	5	5	5	5
0.02	6	6	6	6	5	5	6	6
0.01	6	6	6	7	5	6	7	7
0.001	7	7	7	8	7	7	7	7

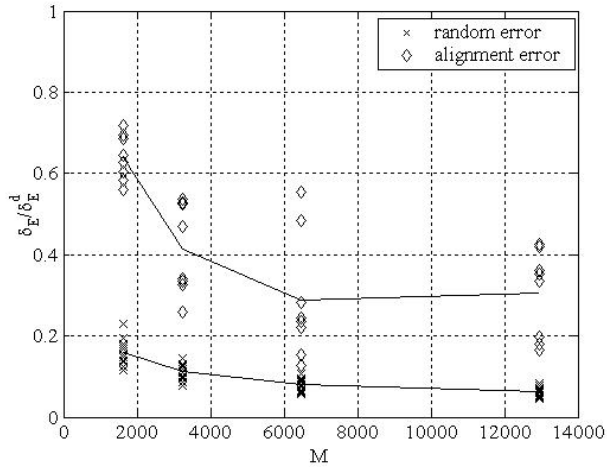

Figure 8. The proportion of SWE error to data error as a function of the number of data.

4. CALCULATION OF THE OPTIMAL TRUNCATION INDEX FROM MEASURED DATA

In the examples explained above, the optimal truncation mode index is determined by comparing the field of SWEs with different truncation indices with the known exact field. A procedure of this kind cannot be applied to measured radiation pattern data, because the exact field is

Table 2. Optimal truncation mode indices for SWEs calculated from the data with ϕ-alignment error.

M	1620		3240		6480		12960	
example	δ_E^d	N_{opt}	δ_E^d	N_{opt}	δ_E^d	N_{opt}	δ_E^d	N_{opt}
1	0.0162	3	0.0155	4	0.0144	4	0.0146	4
	0.0054	4	0.0072	4	0.0072	4	0.0076	4
2	0.0160	5	0.0199	5	0.0193	5	0.0188	5
	0.0104	5	0.0089	6	0.0097	6	0.0097	6
3	0.0246	5	0.0313	5	0.0301	6	0.0288	5
	0.0155	5	0.0141	6	0.0147	6	0.0150	6
4	0.0163	5	0.0304	5	0.0283	5	0.0280	5
	0.0132	5	0.0136	5	0.0119	6	0.0145	5

not known. However, the results of those examples make it possible to create a method, which can be used when the exact field is not known. The typical behaviour of the modal power distribution of a SWE calculated from inaccurate data suggests that the optimal truncation mode index can be determined from a modal power distribution of a SWE, whose truncation index is higher than the optimal one.

Because the modal power distribution is a discrete function, determined only at integer mode index n, its derivatives cannot be calculated in a usual way. However, numerical derivatives can be calculated using values at integer n. Thus, wherever first and second derivatives are mentioned below, they mean actually the corresponding numerical derivatives.

Regardless of the kr_0 value, the characteristic modal power distribution decreases with slowly increasing rate, when the mode index n is above kr_0 and growing. In other words, at mentioned n values, the first derivative of the characteristic modal power distribution is negative and a decreasing function, and the second derivative is negative and approaching zero at infinity. On the other hand, the power distributions of SWEs calculated from inaccurate data begins to turn away from the corresponding characteristic modal power distribution at a mode index near the optimal truncation index, as explained above. At that point, the distribution has its steepest curvature upwards, that is, the second derivative achieves its maximum. In view of these facts, one can conjecture that the optimal truncation mode index is close to mode indices at which the first derivative of the power distribution of SWE calculated from inaccurate data has its minimum and the second derivative has its maximum.

Due to the irregularity at mode indices above the optimal

truncation index and the discontinuity of the calculated modal power distribution, the first and second derivatives calculated from two and three function values, correspondingly, behave quite arbitrarily. Therefore, it turned out that derivatives that are more applicable were obtained by calculating them from more than the minimum number of function values. The first derivative was obtained from the slope of a straight lines calculated by the least square method from three, four and five adjacent points of the calculated modal power distribution. The second derivative was calculated as a numerical derivative of the corresponding first derivative.

4.1. Method to Find the Optimal Truncation Index

The method to find out the optimal truncation mode index without knowing the exact field of an antenna was developed by comparing the known optimal truncation index with the mode indices where the first and second numerical derivatives of the calculated modal power distribution have their respective minimum and maximum values. The behaviour of the logarithmic modal power distribution near the conjectural optimal truncation index was also utilised.

The method consists of the following procedure:

- Input data: complex field values of θ- and ϕ-components at M different directions.
- Calculate the SWE with truncation index $N = \min\left\{n_\phi, n_\theta, \sqrt{M+1} - 1\right\} + 4$.
- Calculate the logarithmic modal power distribution for the obtained SWE.
- Calculate the first- and second derivatives for the logarithmic modal power distribution.
- Find integer mode indices n'_l where the first derivatives obtained from four and five values ($l = 4, 5$ correspondingly) have their minimum. n'_4 must be rounded upwards.
- Find integer mode indices n''_l where the second derivatives obtained from four, five and six values have their maximum. n''_4 and n''_6 must be rounded downwards.
- Set $N_{opt} = \min\{n''_5, n''_6\}$.
- If $N_{opt} > n'_5 + 2$ and $N_{opt} > n''_4$, set $N_{opt} = N_{opt} - 1$.
- If $\dfrac{1}{3}\displaystyle\sum_{n=N_{opt}+1}^{N_{opt}+3} P(n)[dB] > P(N_{opt})[dB]$, set $N_{opt} = N_{opt} - 1$.

- If $N_{opt} = n''_5 - 1$, $N_{opt} < n''_4$, $N_{opt} \leq n'_5 + 1$ and $N_{opt} \leq n'_4$, set $N_{opt} = N_{opt} + 1$.

This procedure finds the best or second best value for the optimal truncation index in all the examples described above. The error of a calculated SWE increases extremely slowly near the best possible truncation index as can be seen in Section 3.2. Thus choosing the second best truncation index does not much degrade the accuracy of the expansion, and so the procedure can be regarded as satisfactory for all practical purposes.

The procedure has been tested for error-free data when the truncation index was limited by the number of ϕ-cuts or θ-values. When the number of ϕ-cuts is smaller, the procedure finds the optimal truncation index equally well as in the examples where the truncation index was limited by the errors of the data. In the case of smaller number of θ-values the procedure sometimes fails, because in that case the overlong SWE, calculated at the beginning of the procedure, behaves irregularly and does not follow the characteristic modal power distribution below the optimal truncation index. If the expansion is calculated with a truncation index equal to the best possible index, the modal power distribution agrees well with the characteristic one and, if the truncation index is increased only by one, solely the last value diverges from the characteristic modal power distribution. This feature can be used to develop a procedure which works well in a case where the truncation index is limited by the number of θ-values, but since such case seldom occurs in real measurements or simulations, it is not done here.

4.2. Application to Measured Radiation Patterns

The developed method has been applied to measured radiation patterns of two different antennas. The first antenna consists of two half-wave dipoles above a ground plane and the second is a monopole antenna on a metal box. The antennas are shown in Figure 9 with the used measurement co-ordinates. The radiation patterns were measured on 18 ϕ-cuts ($\phi = 0°, 10° \ldots 170°$) with 90 θ-values ($\theta = 1°, 3° \ldots 179°$). In the chosen co-ordinates kr_0 was 2.84 (only the dipoles included) or 4.64 (the ground plane is included) for the first and 4.18 for the second antenna.

The modal power distributions with $N = 18$ for the measured radiation patterns are shown in Figure 10, together with the optimal truncation indices obtained by the developed method. The figure shows that the modal power distributions calculated from the actual measured radiation pattern data behave similarly as the ones

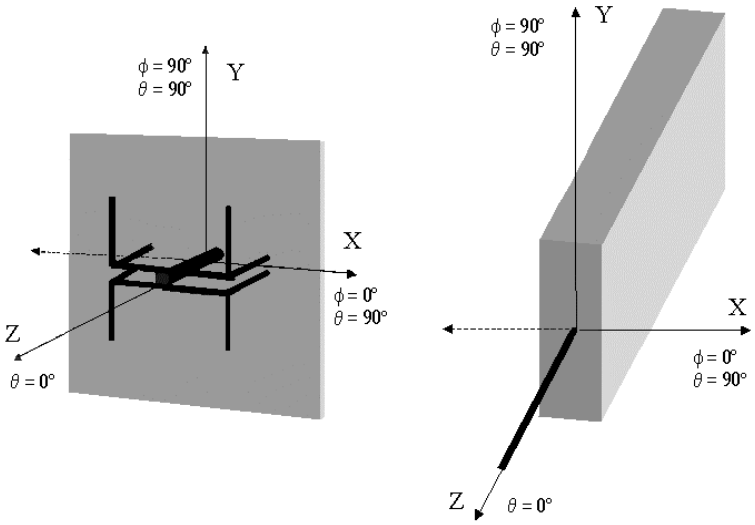

Figure 9. Geometries of the antennas placed in the co-ordinates used in the antenna pattern measurements.

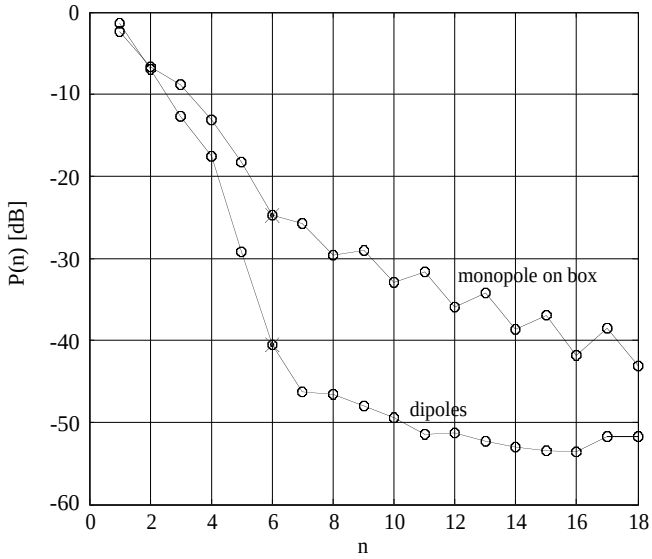

Figure 10. Modal power distributions calculated from measured radiation patterns for two different antennas. The optimal truncation indices calculated by the developed method are marked with crosses.

calculated from the simulated examples. Thus, one can presume that the method to find the optimal truncation index works also with real measurement data. Besides, the obtained optimal truncation indices seem to be appropriately situated.

5. CONCLUSIONS

In this paper, error of the radiation pattern data was decreased by finding the optimal truncation index for spherical wave expansion calculated from an inaccurate data. Four analytical examples of known radiation pattern examples were examined, to which random and ϕ-alignment errors were added. The SWEs, calculated with the optimal truncation index, were seen to be significantly more accurate than the original data. The random error was reduced drastically: about 80–95% of the initial error was removed. With the alignment error, the effect was less significant and more varying: 30–80% of the error was eliminated.

A procedure was developed to determine the optimal truncation index from the modal power distribution of a SWE using the knowledge obtained from the analytical examples. Since it is not necessary to know the exact field, the procedure is applicable to any measured or simulated data.

REFERENCES

1. Hansen, J. E. (Ed.), *Spherical Near-Field Antenna Measurements*, IEE Electromagnetic Waves Series 26, Peter Peregrinus Ltd., London, United Kingdom, 1988.
2. Thal, H. L. and J. B. Manges, "Theory and practise for a spherical-scan near-field antenna range," *IEEE Trans. on Antennas and Propagation*, Vol. 36, No. 6, 815–821, June 1988.
3. Wiscombe, W. J., "Improved Mie scattering algorithms," *Applied Optics*, Vol. 19, No. 9, 1505–1509, May 1980.
4. Koivisto, P. K., "Analytical solution for characteristic modal power distribution and truncation limit for spherical wave expansion of antenna radiation pattern," *Journal of Electromagnetic Waves and Applications*, Vol. 16, No. 9, 1307–1328, 2002.
5. *IEEE Standard Test Procedures for Antennas*, ANSI/IEEE Std 149-1979, The Institute of Electrical and Electronics Engineers, Inc.
6. Leatherwood, D. A. and E. B. Joy, "Plane wave, pattern

subtraction, range compensation," *IEEE Trans. on Antennas and Propagation*, Vol. 49, No. 12, 1843–1851, December 2001.

7. Dich, M. and H. E. Gram, "Alignment errors and standard gain horn calibrations," *Proc. of the 19th Meeting and Symposium of the Antenna Measurement Technique Association*, 425–430, Boston, MA., USA, November 17–21, 1997.
8. Black, D. N. and E. B. Joy, "Test zone field compensation," *IEEE Trans. on Antennas and Propagation*, Vol. 43, No. 4, 362–368, April 1995.
9. Jofre, L., E. B. Joy, and R. Wilson, "Antenna pattern correction for range reflections," *Proc. AMTA*, 1987.
10. Harrington, R. F., *Time-Harmonic Electromagnetic Fields*, Mc Graw-Hill, 1961.
11. Stratton, J. A., *Electromagnetic Theory*, 1st ed., McGraw-Hill, New York and London, 1941.
12. Papas, C. H., *Theory of Electromagnetic Wave Propagation*, Dover Publications, Inc., New York, 1988.

Päivi Koivisto received the degrees of Dipl.Eng., Lic.Tech. and Dr.Tech. from the Helsinki University of Technology in 1985, 1992 and 1994, respectively. Presently she is with the VTT Information Technology. Her interest range from antennas to numerical and analytical electromagnetics.